

Supporting Information

Kaneko et al. 10.1073/pnas.1013866107

SI Materials and Methods

Optical Imaging of Intrinsic Signals. Monocular deprivation (MD) was performed as described (1), except that 2–3% isoflurane in oxygen was used for anesthesia. The lid of the right eye (contralateral to the imaged hemisphere) was sutured shut at P24–26, 1 d after the first (baseline) imaging session; subsequent imaging sessions were then performed in the same individuals after 1, 3, and 6 d of MD. All recordings were made from V1. Extra care was taken to minimize the exposure of the deprived eye to light during the second and third imaging sessions. To examine recovery from MD, another set of mice was imaged immediately before MD, after 5 d of MD, and 1 d after restoring vision to the deprived right eye (following 6 d of MD) either by simply removing the suture (binocular vision, BV), or by reversing the lid suture (reverse occlusion, RO).

Repeated optical imaging of intrinsic signals and quantification of ocular dominance were performed as described (2). Briefly, during recording, mice were anesthetized with 0.7% isoflurane in oxygen applied via a home-made nose mask, supplemented with a single intramuscular injection of 20–25 μ g chlorprothixene. We monitored the concentration of isoflurane by using an Ohmeda 5250 RGM (Datex-Ohmeda) throughout each imaging session. Images were recorded transcranially; the scalp was sutured closed at the end of each session and reopened at the same location in subsequent sessions. Intrinsic signal images were obtained with a Dalsa 1M30 CCD camera (Dalsa) with a 135 \times 50 mm tandem lens (Nikon) and red interference filter (610 \pm 10 nm). Frames were acquired at a rate of 30 frames/s, temporally binned by 4 frames, and stored as 512 \times 512 pixel images after binning the 1024 \times 1024 camera pixels by 2 \times 2 pixels spatially. The visual stimulus for recording the binocular zone, presented on a 40 \times 30 cm monitor placed 25 cm in front of the mouse, consisted of 2°-wide bars, which were presented between -5° and 15° on the stimulus monitor (0° = center of the monitor aligned to center of the mouse) and moved continuously and periodically upward or downward at a speed of 10°/s. The phase and amplitude of cortical responses at the stimulus frequency were extracted by Fourier analysis as described (3). Response amplitude was an average of at least four measurements. Ocular dominance index was computed as described (2). Mice were kept under standard housing conditions with free access to food and water between recordings. For assessment of retinotopy, intrinsic signal images were acquired by using a full-screen bar stimulus as described (3). Response area was calculated by selecting pixels with response amplitudes larger than 30% of the maximum value. The map scatter index was computed as described (4).

Extracellular Single-Unit Recording in Vivo. Baseline response properties of visual cortical neurons were examined in mice with normal visual experience at P28–35. Plasticity at the single-unit level was investigated at P28–33 in mice that either underwent no visual deprivation, 3 d of MD, or 1 d of RO after 5 d of MD. Data acquisition, visual stimuli, and spike analyses were performed as described (5) with small modifications. Mice were anesthetized with isoflurane (1.5–2% for surgical preparation and 0.7% for recording) in oxygen supplemented with 0.2 mg of chlorprothixene. A custom stainless-steel headplate was cemented to the skull to allow head fixation and a small craniotomy (<1 mm diameter) was made over the binocular area of V1 (3 mm lateral to the sagittal suture and 0.5 mm anterior to lambda). A silicon multisite electrode with a tetrode configuration (model a2 \times 2-tet-3mm-150–121; Neuronexus Technologies) was inserted at an angle of $\approx 45^\circ$ relative to the cortical surface,

to a depth of <400 μ m below the cortical surface to record cells in layer 2/3. Visual stimuli were generated in Matlab (MathWorks) by using the Psychophysics Toolbox extensions and displayed on a monitor placed 25 cm in front of the mouse, subtending ≈ 60 – 75° of visual space. To measure the responsiveness of cells, we presented drifting sinusoidal gratings of 1.5-s duration at 100% contrast, with a temporal frequency of 2 Hz, spatial frequency of 0.01, 0.02, 0.04, 0.08, 0.16, 0.32, and 0 cycles per degree, in 12 evenly spaced directions. The stimulus conditions were randomly interleaved, and a gray blank condition was included to estimate the spontaneous firing rate. Signals were acquired by using a System 3 workstation (Tucker-Davis Technologies) and analyzed with custom software in Matlab. Unit clustering and spike waveform analysis were performed as described (5). The average spontaneous firing rate for each unit was calculated by averaging the rate over all blank condition presentations. Responses to each orientation and spatial frequency were calculated by averaging the spike rate during the 1.5-s presentation and subtracting the spontaneous firing rate. The preferred orientation was determined by averaging the response across all spatial frequencies and calculating half the complex phase of the value $\frac{\sum F(\theta)e^{2i\theta}}{\sum F(\theta)}$. Given this fixed preferred orientation θ_{pref} , the tuning curve was fitted with the sum of two Gaussians centered on θ_{pref} and $\theta_{\text{pref}} + \pi$, of different amplitudes A_1 and A_2 but equal width θ , with a constant baseline B . From this fit, we calculated an orientation selectivity index (OSI) as the depth of modulation from the preferred orientation to its orthogonal orientation $\theta_{\text{ortho}} = \theta_{\text{pref}} + \pi/2$, as $(R_{\text{pref}} - R_{\text{ortho}})/(R_{\text{pref}} + R_{\text{ortho}})$. Receptive field size was calculated from responses to full-field light bars sweeping across the visual field in 16 evenly spaced directions. The responses from eight sweeps were binned at 100 ms and used to construct firing rate as a function of bar position. This response profile was fitted with a 2D Gaussian, with independent widths θ_x and θ_y , and RF radius was calculated by averaging the half-width at half-maximum of the two axes of the Gaussian fit. Ocular dominance index was calculated as $(R_{\text{contra}} - R_{\text{ipsi}})/(R_{\text{contra}} + R_{\text{ipsi}})$, where R_{contra} and R_{ipsi} were response rates to a drifting grating stimulus of preferred orientation and spatial frequency presented to the contralateral and ipsilateral eyes, respectively. Note that the eyelid suture was done on the eye contralateral to the hemisphere from which recordings were performed.

Brain Slice Preparation and Whole Cell-Recording. P26–P30 H-ras^{G12V} mice and WT littermates were killed by cervical dislocation and decapitated, and brains were rapidly removed into ice-cold dissection buffer (108 mM choline-Cl, 3 mM KCl, 26 mM NaHCO₃, 1.25 mM NaH₂PO₄, 25 mM D-glucose, 3 mM Na-pyruvate, 1 mM CaCl₂, 6 mM MgSO₄, 285 mM mOsm) bubbled with 95% O₂/5% CO₂. Four hundred micrometer-thick coronal slices were cut through V1 by using a VT1000S microtome (Leica Microsystems). Brain slices were incubated in a submerged chamber in artificial cerebrospinal fluid (ACSF; 119 mM NaCl, 3.5 mM KCl, 1 mM NaH₂PO₄, 10 mM D-glucose, 2 mM CaCl₂, 1 mM MgSO₄, 300 mM mOsm) bubbled with 95% O₂/5% CO₂, at 32 $^\circ$ C for 45 min, and then at room temperature until recording.

Slices containing the binocular zone of V1 were selected and L2/3 pyramidal neurons were identified under infrared differential interference contrast (IR-DIC) optics by using an Olympus BX50WI microscope. Recording pipettes (10–15 M Ω for LTP experiments to reduce dialysis of the postsynaptic neuron, 5–8 M Ω for all other recordings) contained 130 mM KMeSO₄, 8 mM NaCl, 2 mM KH₂PO₄, 2 mM D-glucose, 10 mM Hepes, 4 mM Mg-ATP,

7 mM phosphocreatine, 0.3 mM GTP, 0.5 mM ADP at pH 7.30, 285 mOsm. Recorded neurons had resting membrane potentials ≤ -70 mV, not corrected for the liquid junction potential of +8 mV. Access resistance and pipette capacitance were fully compensated (Multi-clamp 700B; Molecular Devices). Recordings were discarded if membrane potential depolarized by >5 mV or access resistance increased by $>20\%$. The identity of pyramidal neurons was confirmed by their regular spiking behavior. Action potentials were low-pass filtered at 10 kHz, extracellularly evoked EPSPs at 6 kHz and mEPSPs at 3 kHz, and data were digitized at 10–20 kHz (CED1401 and micro1401) and recorded by using Signal v1.85 or 4.05 (all Cambridge Electronic Devices). Intrinsic excitability was assessed by injection of square depolarizing current pulses. Input resistance was monitored throughout recordings by injection of square hyperpolarizing current pulses.

LTP and Short-Term Synaptic Dynamics. A monopolar tungsten extracellular stimulating electrode (0.5 M Ω ; Intracel) was positioned in L4 by using a 5 \times objective, and the position was verified under IR-DIC by using a 40 \times objective. Recorded neurons were radially above the stimulating electrode. Stimulation intensity (0.8–4.0 V, 0.2-ms pulses) was set to produce a 3–6 mV monosynaptic EPSP in the postsynaptic neuron. Neurons were stimulated (Master8; AMPI) with trains of eight pulses at 20 Hz with 15 s between trains to assess short-term synaptic dynamics. Recordings of LTP experiments consisted of pairs of pulses at 20 Hz, with 10 s between trials. A stable baseline was recorded before LTP was induced by pairing a just-suprathreshold 2–3 ms somatic current pulse with a single presynaptic stimulus (prepost interval of +5 ms). Four trains of 50 paired stimuli at 2 Hz were delivered at 0.025 Hz. Responses were recorded for 1 h after LTP induction. Monosynaptic EPSP amplitudes were measured as the difference between baseline and peak response amplitude. Significant potentiation was defined as an increase in EPSP amplitude of $\geq 15\%$ between baseline and 50–60 min after LTP induction. PPR was defined as the EPSP2/EPSP1 amplitude ratio. The change in PPR after LTP was assessed for individual neurons by comparing values during the baseline period before LTP induction with those recorded 50–60 min after LTP induction by using Student's *t* tests. Initial EPSP (EPSP1) amplitude was similar in WT (4.5 ± 0.3 mV) and H-ras^{G12V} (4.3 ± 0.3 mV; $P = 0.71$, *t* test, $n = 25$ per group) mice.

mEPSPs. For experiments to assess the effect of MD, the lid of the left eye was sutured shut at P25–26 under isoflurane anesthesia (2% in O₂, 0.6 L/min). After 3 or 6 d of MD, the integrity of the deprivation was checked, and brain slices were prepared from the right hemisphere as described above. mEPSPs were isolated by bath application of 1 μ M tetrodotoxin, 100 μ M picrotoxin, and 50 μ M D-AP5 (all Tocris). Action potential blockade was confirmed by injection of square depolarizing current pulses (1 nA, 500 ms). At least 50 mEPSPs per cell were analyzed by using the Mini Analysis Program (Synaptosoft). The threshold for detection of mEPSPs was set at 2.5 times the root mean square of baseline noise (6, 7). mEPSPs with a 10–90% rise time <1 ms or >5 ms were excluded from analysis. There was no significant difference in root mean square noise between experimental groups ($P = 0.52$ for effect of genotype, $P = 0.21$ for effect of MD, $P = 0.14$ for interaction between factors; two-way ANOVA). No neurons exhibited a negative correlation between mEPSP amplitude and mEPSP rise time.

Rate of Use-Dependent Blockade of NMDARs by MK-801. NMDAR-mediated responses were isolated in magnesium-free ACSF containing 20 μ M CNQX. An extracellular electrode in L4 delivered stimuli at 0.1 Hz. Stimulus voltage ($P = 0.50$, *t* test) and NMDAR-mediated response amplitude ($P = 0.74$, *t* test) were similar in WT and H-ras^{G12V} groups. After recording a stable baseline, 10 μ M MK-801 [(5S,10R)-(+)-5-methyl-10,11-dihydro-

5H-dibenzo[a,d]cyclohepten-5,10-imine maleate] was washed onto the slice for 10 min without stimulation. Stimulation (0.1 Hz) was then resumed, and ≥ 100 trials were recorded. For each neuron, the decay in response amplitude over time was fitted with a double exponential function (8, 9) of the form $y = ae^{-bx} + ce^{-dx}$ by using Sigmaplot (Systat). Single exponential fits to the decay phase of NMDAR-mediated EPSPs were of the form $y = y_o + ae^{-bx}$, and all had $R > 0.995$ and $P < 0.001$ for each coefficient. The mean time constant of the rate of blockade was calculated for each neuron by using the time constants of the fast- and slow-component exponential fits and the proportion of synapses fitted by each function.

Statistics. Data are described by their mean \pm SEM. For in vitro data, normally distributed datasets with equal variances were analyzed with paired or unpaired *t* tests and ANOVAs. Other data sets were compared with Mann–Whitney tests, all using GraphPad Prism 2.01 or SigmaStat 3.1. Kolmogorov–Smirnov tests (Matlab) were used to compare distributions. LTP data were analyzed by using a two-way ANOVA to assess the role of genotype and time after LTP induction (as 10-min epochs; $P = 0.998$ for time epoch, $P = 0.97$ for interaction between genotype and time epoch). Short-term dynamics were also analyzed with a two-way ANOVA to determine the effects of genotype and stimulus number ($P = 0.002$ for stimulus number, $P = 0.999$ for interaction between stimulus number and genotype). All tests were two-tailed, and α was set at 0.05. Response magnitudes and ocular dominance index (ODI) data obtained from intrinsic signal imaging experiments were analyzed by using repeated measures ANOVAs to assess changes from baseline values, as well as one-way ANOVAs to compare genotypes, both with Bonferroni corrections for multiple comparisons. Extracellular single-unit spike data were analyzed by using Mann–Whitney *u* tests and Kolmogorov–Smirnov tests.

SI Data

Basal Response Properties of Primary Visual Cortex in H-ras^{G12V} Mice. To determine whether H-ras^{G12V} expression affects the basal response properties of V1, we examined functional retinotopic organization and global responsiveness by using intrinsic signal optical imaging. The quality of retinotopic maps (Fig. S2A and Fig. S3), the response magnitude (Fig. S2B), and the area of cortex responding to visual stimuli presented to the central visual field (Fig. S2C) were statistically indistinguishable between H-ras^{G12V} and WT mice.

Next, we examined response properties at the single-unit level by recording extracellularly from upper layer neurons at P28–35 using silicon microprobes in a tetrode configuration. We focused our attention on single units in the upper layers (2, 3, and 4) with “broad” spikes, which are thought to originate from excitatory neurons (5, 10). Earlier work showed such neurons to be highly selective for visual stimuli (5). Our studies in vitro described below focused on the same population of neurons. Broad-spiking units in the upper layers constituted $\approx 80\%$ of neurons in both WT and H-ras^{G12V} mice. All aspects of visual responses were identical in WT and H-ras^{G12V} mice, including response rates evoked by an optimal drifting grating stimulus (Fig. S2D), receptive field size (Fig. S2E), orientation selectivity (Fig. S2F), orientation tuning width (Fig. S3C), and spatial frequency tuning (Fig. S3D). The H-ras^{G12V} animals did, however, have a somewhat higher level of spontaneous activity in the absence of a visual stimulus (Fig. S2G). Thus, single-unit recordings in H-ras^{G12V} mice revealed normal development of the characteristic, highly specific receptive fields in the mouse visual cortex.

Comparison of Effects of MD Starting at P24–26 with MD Starting at P28–29. In the present experiments, MD was carried out beginning at P25–26 (Fig. 1) or P24–25 (Fig. 2), whereas previous single-unit studies in C57Bl6 wild-type mice placed the peak of the

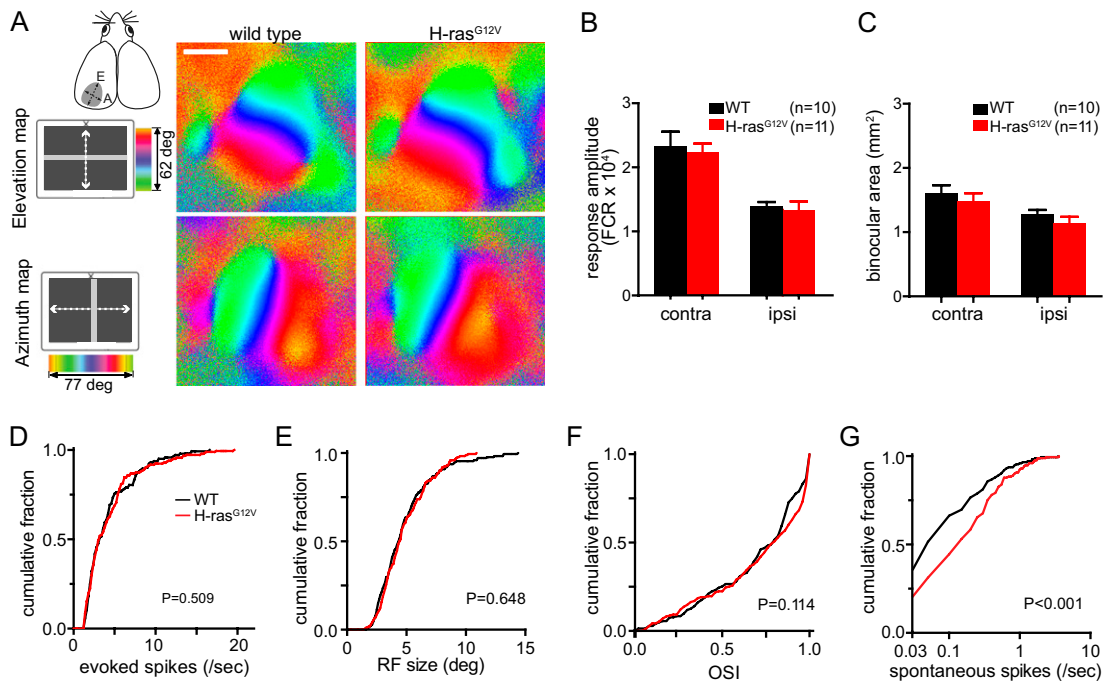


Fig. S2. Basal response properties of the primary visual cortex in H-ras^{G12V} mice are largely normal. (A–C) Intrinsic signal imaging. (A) Examples of visual cortical maps revealed by intrinsic signal optical imaging of responses to presentation to the contralateral eye of a periodically sweeping horizontal bar (elevation maps; *Upper*) or vertical bar (azimuth maps; *Lower*). The bar position that elicited the largest intrinsic signal at each pixel is color-coded as shown. (Scale bar: 1 mm.) (B) Intrinsic signal amplitude in the binocular area of V1 in response to contralateral or ipsilateral eye stimulation with a 20°-long horizontal bar sweeping upward or downward in the central visual field. (C) Cortical area responding to contralateral or ipsilateral eye stimulation. Data are shown as mean \pm SEM. No statistical differences were detected between genotypes ($P = 0.45$ response amplitude—contralateral; $P = 0.52$ response amplitude—ipsilateral; $P = 0.53$ binocular area—contralateral; $P = 0.25$ binocular area—ipsilateral; two tailed t tests; WT 10 mice, H-ras^{G12V} 11 mice). (D–G) Extracellular single-unit recording in WT (black) and H-ras^{G12V} (red) mice. (D) Peak firing rate in response to a drifting grating with an optimal orientation and spatial frequency, presented to the contralateral eye. (E) Orientation selectivity computed from responses to drifting gratings of 16 different directions. (F) Receptive field size in degrees computed from responses to a 2°-thick bar sweeping across the 77° \times 62° visual field. (G) Spontaneous firing rate; plot shows that 36% of WT and 20% of H-ras^{G12V} cells had spontaneous rates <0.03 spikes/s (firing 0 spikes in 32 s). All are presented as cumulative frequency distributions. P values shown are from Kolmogorov–Smirnov tests. WT 143 units in three mice; H-ras^{G12V} 183 units in four mice.

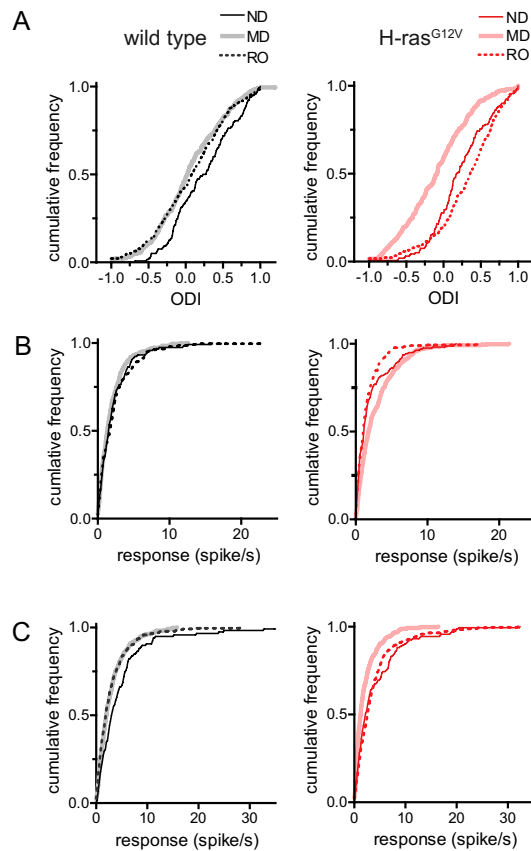


Fig. S5. Accelerated plasticity in H-ras^{G12V} mice assayed with single-unit recordings. Cumulative distributions for the data shown in Fig. 3 as mean \pm SEM. *Left* shows data for single units in WT mice; *Right* shows data for H-ras^{G12V} mice. (A) ODI calculated as the difference between peak firing rates for ipsilateral (B) and contralateral (C) responses divided by the sum of the two. (B) Firing rates evoked by an optimal drifting grating stimulus presented to the initially open (ipsilateral) eye. (C) Firing rates evoked by an optimal drifting grating stimulus presented to the initially deprived (contralateral) eye. ND, no visual deprivation; MD, 3 d of MD; RO, 5 d of MD followed by 1 d of RO. Sample size (units, animals); WT: ND (118, 2), MD (222, 4), RO (234, 4); H-ras^{G12V}: ND (160, 3), MD (266, 5), RO (241, 4). Statistical data are shown in Table S1 and S2.

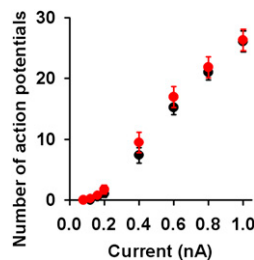


Fig. S6. H-ras^{G12V} expression does not affect the passive membrane properties or intrinsic excitability of L2/3 pyramidal neurons. Intrinsic excitability of L2/3 pyramidal neurons was determined by injecting square depolarizing current pulses of increasing amplitude (500-ms duration). There was no difference between neurons in WT (black) and H-ras^{G12V} (red) mice in terms of either the threshold ($P = 0.31$, t test, $n = 25$ per group) or the slope ($P = 0.80$, t test) of linear regression fits to data from individual neurons. There was also no difference in resting membrane potential (WT, -76 ± 1 mV; H-ras^{G12V}, -75 ± 1 mV; $P = 0.81$, $n = 20$ per group, t test), or input resistance (WT, 53 ± 4 M Ω ; H-ras^{G12V}, 60 ± 5 M Ω ; $P = 0.34$, $n = 20$ per group, t test) between neurons in WT and H-ras^{G12V} mice.

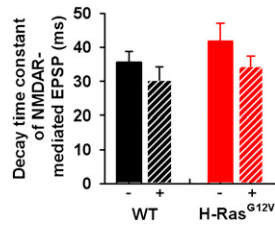


Fig. S7. Decay kinetics of NMDAR-mediated responses is similar in WT and H-ras^{G12V} mice. The decay phases of NMDAR-mediated responses were fitted with single exponential functions. Data are shown as mean \pm SEM. +, presence of 10 μ M MK-801. There was no difference between the decay time constant in WT and H-ras^{G12V} mice ($P = 0.24$ for genotype; $P = 0.14$ for effect of MK-801, $P = 0.80$ for interaction, two-way ANOVA, $n = 10$ per group). Therefore the subunit composition of NMDARs was very similar in WT and H-ras^{G12V} mice, thereby excluding the possibility that differences in NMDAR channel open probability (8, 9) could contribute to the slower rate of use-dependent blockade of NMDARs by MK-801 in H-ras^{G12V} mice (Fig. 5 A–C).

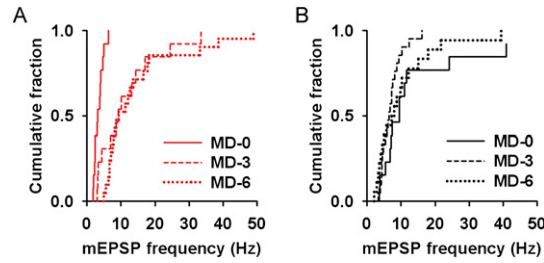


Fig. S8. Effect of MD on distribution of mEPSP frequencies in WT and H-ras^{G12V} mice. (A) Distribution of mEPSP frequency in neurons in H-ras^{G12V} mice before or after 3 or 6 d of MD. (B) Distribution of neurons in WT mice before or after 3 or 6 d of MD.

Table S1. Additional statistical tests on in vivo electrophysiology data: Comparison between treatments within genotype

Comparison	WT–closed	WT–open	H-ras ^{G12V} –closed	H-ras ^{G12V} –open
ND vs. MD	0.001	0.773	<0.001	0.032
ND vs. RO	0.002	0.795	0.194	<0.001
ND vs. RO	0.545	0.099	<0.001	0.141

The numbers are P values from Kolmogorov–Smirnov tests on the cumulative frequency distribution of closed-eye responses, open-eye responses, and ODI, as shown in Fig. S5.

Table S2. Additional statistical tests on in vivo electrophysiology data: Comparison between genotypes (WT vs. H-ras^{G12V})

Condition	Closed eye	Open eye	ODI
ND	0.058	0.117	0.575
MD	<0.001	<0.001	0.001
RO	0.024	<0.001	<0.001

The numbers are P values from Kolmogorov–Smirnov tests on the cumulative frequency distribution of closed-eye responses, open-eye responses, and ODI, as shown in Fig. S5.